

COMPUTING MULTIVALUED PHYSICAL OBSERVABLES FOR THE SEMICLASSICAL LIMIT OF THE SCHRÖDINGER EQUATION

SHI JIN, HAILIANG LIU, STANLEY OSHER, AND RICHARD TSAI

ABSTRACT. We develop a level set method for the computation of multivalued physical observables (density, velocity, etc.) for the semiclassical limit of the Schrödinger equation in arbitrary number of space dimensions. The main idea is to evolve the density near an n -dimensional manifold that is identified as the common zeros of n level set functions in phase space. These level set functions are generated from solving the Liouville equation with initial data chosen to embed the phase gradient. Simultaneously we track a new quantity f by solving again the Liouville equation near the obtained zero level set but with initial density as initial data. The multivalued density and higher moments are thus resolved by integrating f along the n -dimensional manifold in the phase directions. It turns out that our method provides a geometrical ansatz for the limiting Wigner equation since the aforementioned function, f , multiplied by a Dirac- δ function applied to the level set function ϕ , solves the same equation as that for the distribution density function exploited in the Wigner approach. The main advantages of this new approach, in contrast to the standard kinetic equation approach using the Liouville equation with a Dirac measure initial data, include: 1) the Liouville equations are solved with L^∞ initial data, and a singular integral involving the Dirac- δ function is evaluated only in the post-processing step, thus avoiding oscillations and excessive numerical smearing; 2) a local level set method can be utilized to significantly reduce the computation in the phase space. These advantages allow us to compute, for the first time, *all* physical observables for multidimensional problems.

CONTENTS

1. Introduction	2
2. Level set equations for multivalued physical observables in the phase Space	6
2.1. Multivalued velocity and phase	6
2.2. Multivalued density	7
3. Numerical Implementation and Results	9
3.1. Numerical procedure	10
3.2. On numerical integration of the moments	13
3.3. Numerical examples	15
4. Conclusion	17
Appendix	18
Acknowledgments	23
References	24

1. INTRODUCTION

In this paper we are concerned with numerical computation of the (multi-valued) physical observables to the linear Schrödinger equation

$$(1.1) \quad i\varepsilon\partial_t\psi^\varepsilon = -\frac{\varepsilon^2}{2}\Delta\psi^\varepsilon + V(x)\psi^\varepsilon, \quad x \in \mathbb{R}^n,$$

subject to highly oscillatory wave function as initial data

$$(1.2) \quad \psi(x, 0) = A_0(x) \exp(iS_0(x)/\varepsilon).$$

Here V is a given smooth potential, ε is the rescaled Planck constant. In the semiclassical regime, $\varepsilon \ll 1$, the function ψ^ε has $O(\varepsilon)$ wave length, and its associated physical observables become highly oscillatory. Direct numerical simulations of the Schrödinger equation become prohibitively costly since one needs to resolve the oscillations [1, 20]. A natural way to remedy this problem is to use the asymptotic solution, which is the limit of the solution to the Schrödinger equation as $\varepsilon \rightarrow 0$. The classical approach is the WKB (Wentzel-Kramers-Brillouin) method, which uses the following ansatz

$$(1.3) \quad \psi(x, t) = A(x, t) \exp(iS(x, t)/\varepsilon).$$

With this decomposition, the leading order behavior is characterized by two quantities, the phase function S which satisfies the nonlinear eikonal equation, and the amplitude function A which satisfies a transport equation, i.e.,

$$(1.4) \quad \partial_t S + \frac{|\nabla_x S|^2}{2} + V(x) = 0,$$

$$(1.5) \quad \partial_t |A|^2 + \nabla_x \cdot (|A|^2 \nabla_x S) = 0.$$

Since the unknowns in this lowest order WKB system, i.e. the phase and the amplitude, are independent of the small scale, they are, in principle, easier to compute numerically.

However, a well-known drawback of this approach is the lack of a superposition principle when the linear equation (1.1) is replaced by nonlinear ones (1.4)-(1.5). The solution of a nonlinear eikonal equation, in general, develops singularities in finite time. Viscosity solutions were introduced in [6] to mathematically select a unique, single valued weak solution. Unfortunately, this class of weak solutions is not appropriate in treating linear wave propagation problems. Instead, multivalued solutions that are determined by the stationary phases and the corresponding to crossing waves, are the physically relevant ones. Constructing such multivalued solutions is the subject of study in this paper. Our goal is to develop an efficient numerical

method capable of computing the multivalued quadratic physical observables, including position density and velocity. An essential ingredient in our approach is the level set function.

Let $u = \nabla_x S$ denote the phase gradient. Then for smooth solutions, the gradient of the eikonal equation (1.4) satisfies the forced Burgers' equation

$$(1.6) \quad \partial_t u + u \cdot \nabla_x u + \nabla_x V = 0.$$

This equation, coupled with the transport equation (1.5), yield the pressureless gas equation for density $\rho = |A|^2$ and velocity u :

$$(1.7) \quad \partial_t \rho + \nabla_x \cdot (\rho u) = 0,$$

$$(1.8) \quad \partial_t \rho u + \nabla_x (\rho u u) + \rho \nabla_x V(x) = 0.$$

Thus we shall refer the quantity $u = \nabla_x S$ as either the phase gradient or the velocity.

A level set method was introduced in [4, 16] to compute the multivalued solution to the forced Burgers' equation (1.6), and more generally, the multivalued solution of general quasilinear PDEs. In this method, the velocity u is embedded into an n -dimensional manifold, which corresponds to the intersection of n zero level set functions, each satisfying the Liouville equation

$$(1.9) \quad \partial_t \phi + p \cdot \nabla_x \phi - \nabla_x V \cdot \nabla_p \phi = 0.$$

In general, equation (1.4) is not homogeneous of degree one in the gradient, and consequently, the phase value S is not a constant along the characteristics. Therefore, if one is interested in the values of S , simply solving (1.9) is not enough. To compute the multivalued phase S , satisfying the Hamilton-Jacobi equation

$$(1.10) \quad \partial_t S + H(x, \nabla_x S) = 0, \quad x \in \mathbb{R}^n,$$

which includes (1.4) with $H(x, p) = |p|^2/2 + V(x)$, the authors in [4] suggest solving an additional level set function in the augmented space (x, p, z) with $z = S(t, x)$.

This is the context of our present paper. We are interested in computing the density and other quadratic physical observables, in addition to the multivalued velocity and phase, in the level set framework. In particular, given the multivalued velocity, we need to solve the continuity equation (1.7), which is a linear transport equation with discontinuous and multivalued (!) coefficient. Clearly, at points where physical solutions for the velocity are multivalued, the corresponding density will also become multivalued. Moreover, the density may become unbounded at the boundaries

of each single valued branch of the multivalued solution. This is a phenomenon that arises in the modeling of sticky particles (by the pressureless gas equations) that is related to the formation of large scale structures in the universe [32].

We sketch our main idea using the one dimensional Schrödinger equation as an example. We use a level set function ϕ in the phase space, $(x, p) \in \mathbb{R}^2$ with $p = u$, to track the bicharacteristics. As shown in [4, 16], the scalar level set function $\phi(t, x, p)$ satisfies a linear *Liouville equation*

$$(1.11) \quad \partial_t \phi + p \phi_x - V_x \phi_p = 0.$$

The zero level set of this function, initiated as $p - \partial_x S_0(x)$, forms a one-dimensional manifold in (x, p) space. We need to perform integration along this manifold to obtain the physical observables.

We show that the WKB system (1.4)-(1.5) can be rewritten in phase space as

$$(1.12) \quad \partial_t S + p \partial_x S - \partial_x V \partial_p S = p^2/2 - V(x),$$

$$(1.13) \quad \partial_t \rho + p \partial_x \rho - \partial_x V \partial_p \rho = \rho \frac{\partial_x \phi}{\partial_p \phi}.$$

As we mentioned earlier, one strategy to resolve S is to look at the graph of the function $z = S(x, t)$ in the whole domain and project the phase value onto the manifold $\{\phi = 0\}$, see[4]. In this work, we propose to track the new quantity

$$f(t, x, p) := \rho(t, x, p) |\partial_p \phi|,$$

for density calculations, and show that this new quantity f satisfies the Liouville equation

$$\partial_t f + p \partial_x f - \partial_x V \partial_p f = 0, \quad f(0, x, p) = \rho_0(x).$$

I.e. *the concentration singularities in ρ are canceled out by the zeros of $\partial_p \phi$!* This is one of the main results in the paper, and seems new to the best of our knowledge.

The combination of the level set function ϕ and the function f enables us to compute the desired physical observables, for example density and velocity, via integrations against a delta function concentrating on the zero of the level set function:

$$(1.14) \quad \bar{\rho}(x, t) = \int f(t, x, p) \delta(\phi) dp,$$

$$(1.15) \quad \bar{u}(x, t) = \int p f(t, x, p) \delta(\phi) dp / \bar{\rho}.$$

We point out that our proposed approach recovers that by the Wigner transform. By defining the distribution density

$$\eta(x, p, t) := f(x, p, t)\delta(\phi),$$

we can show that η satisfies the following Liouville

$$(1.16) \quad \partial_t \eta + p\eta_x - V_x \eta_p = 0, \quad \eta(0, x, p) = \rho_0(x)\delta(p - u_0(x)).$$

This is the same equation (and initial condition) as that which can be derived from the semiclassical limit of the Schrödinger equation (1.1) with initial data (1.2) by using the Wigner distribution, where η is the density distribution of the limit of the Wigner function as $\varepsilon \rightarrow 0$ [10, 11, 18].

Of course, one can directly solve (1.16) to obtain the physical observables by taking moments (integrating with respect to p). This was done for the Vlasov-Poisson systems in [17]. There are two numerical disadvantages with this approach. First, the equation, defined in the phase space, demands prohibitive amount of computer memory due to high dimensionality. Second, even without the high dimensionality problem, one still needs to numerically approximate the delta function. In fact, given the initial value for η in (1.16), the density contains one delta function (for a single valued solution) or superposition of several delta functions in p , see [15, 26]. Numerically, a "regularized" function has to be used to approximate this type of distributional initial data. It is then foreseeable that this regularized functions with "narrow spikes" is likely to be smeared out by the numerical viscosity of the shock capturing methods used to solve the Liouville equation.

Previous attempts to avoid the difficulties arising in the high dimension problem focused on moment methods. There are two techniques available in the literature. One way is to obtain the closure system based on Dirac delta-type initial data. see [3, 7, 13, 15]. The other approach, proposed by Brenier and Corrias [2], is based on (1.16), and the system arising from (1.16) is closed using Heaviside-type initial data, see [7, 8, 12]. Moment methods require careful numerical solutions to weakly hyperbolic systems, and become difficult, if not impossible, when the number of phases is large, and in higher space dimensions.

In the level set framework, the high dimensionality that comes from working in the phase space can be compensated by the local level set approach in the same manner as in e.g., [4, 5, 22, 24]. If one uses this approach, the total computational complexity reduces to that comparable to a computation in the physical space. In comparison, the corresponding localized algorithm for solving (1.16) has not been reported. In contrast to tracking singular data in the direct methods for (1.16), our new level set

methods solve the Liouville equations for ϕ and f respectively with L^∞ initial data. Due to linearity of the Liouville equation, ϕ and f remain as smooth as their initial values. *We do not approximate the delta function until $\bar{\rho}$ or other higher moments are evaluated.* This approach significantly enhances the quality of the numerical solutions when compared to a direct Liouville solver based on (1.16). In other words, the approach proposed in this paper provides a more efficient and accurate numerical method for (1.16) than numerically solving (1.16) directly (this will be demonstrated numerically in Section 3). Finally, when compared to the moment methods, our method automatically computes all the multivalued phases using a set of linear convection equations (The Liouville equations), and is thus much more robust.

This paper is organized as follows. Section 2 is devoted to a derivation of the equation for the new quantity f as well as the justification of the integration procedure. In Section 3 we discuss our numerical procedures for computing multivalued density and the momentum and present some numerical results. In particular, we discuss the strategies on evaluating singular integrals (1.14) and (1.15). Finally, we give an alternative justification of our new level set method in the Appendix.

2. LEVEL SET EQUATIONS FOR MULTIVALUED PHYSICAL OBSERVABLES IN THE PHASE SPACE

In essence, the first part of our method consists of tracking the bicharacteristics of (1.4) or (1.6) in the phase space, using the level set method developed in [4, 16]. The bicharacteristics for the phase equation (1.4), or (1.6), are governed by the Hamiltonian system

$$(2.1) \quad \frac{dx}{dt} = p, \quad x(0) = \alpha,$$

$$(2.2) \quad \frac{dp}{dt} = -\nabla_x V(x), \quad p(0) = \nabla_x S_0(x) \equiv u_0(x)$$

In this section we first review our previous level set equations for multivalued velocity and phases, and then develop a new method for computing multivalued density and other physical observables that are higher order moments of the solution of the Liouville equation (1.16).

2.1. Multivalued velocity and phase. As we mentioned in the introduction, the multivalued phase gradient or velocity may be implicitly realized as the zero vector level set of the function $\phi(t, x, p) \in \mathbb{R}^n$, satisfying the Liouville equation

$$(2.3) \quad \partial_t \phi + p \cdot \nabla_x \phi - \nabla_x V \cdot \nabla_p \phi = 0,$$

subject to initial data $\phi(0, x, p) = p - \nabla_x S_0(x)$ or its smooth approximation. Such a zero level set represents a n -dimensional manifold in phase space $(x, p) \in \mathbb{R}^n$ and gives implicitly the multivalued phase gradient; i.e.

$$\phi(t, x, p) = 0, \quad p = \nabla_x S.$$

Note that each level set function ϕ is an L^∞ function in a bounded domain if the initial velocity u_0 is bounded.

The phase S can not be obtained from solving the Liouville equation (2.3) since S is not preserved along the Hamilton dynamics. Instead in the phase space (x, p) the phase solves a forced transport equation

$$(2.4) \quad \partial_t S + p \cdot \nabla_x S - \nabla_x V \cdot \nabla_p S = \frac{|p|^2}{2} - V(x).$$

In [4] the authors solve this linear transport equation and then project the obtained phase value onto the n -dimensional manifold $\phi = 0$, and thus resolve the multivalued phase in the physical space. Consult [4, 19] for further details.

2.2. Multivalued density. Similar to (2.4), we obtain the evolution equation for density in the phase space

$$(2.5) \quad \partial_t \rho + p \cdot \nabla_x \rho - \nabla_x V \cdot \nabla_p \rho = \rho G,$$

where G , evaluated as $-\Delta_x S$, can be expressed as

$$G = \text{Tr}((\nabla_p \phi)^{-1} \nabla_x \phi).$$

Let $Q := \nabla_p \phi(t, x, p)$, we differentiate and obtain

$$\nabla_x \phi + \nabla_p \phi \cdot D^2 S = 0,$$

where $D^2 S$ denotes the Hessian of S . This leads to

$$D^2 S = -Q^{-1} \nabla_x \phi.$$

Therefore in (x, p) space the density satisfies

$$(2.6) \quad \partial_t \rho + p \cdot \nabla_x \rho - \nabla_x V \cdot \nabla_p \rho = \rho \text{Tr}(Q^{-1} \nabla_x \phi)$$

where we have used the fact $\Delta S = \text{Tr}(D^2 S) = -\text{Tr}(Q^{-1} \nabla_x \phi)$. Here the density satisfies a linear homogeneous equation in the phase space, and thus the superposition principle holds and the multivaluedness is “unfolded” in (x, p) space.

One may solve the above density equation coupled with the Liouville equation (2.3) and then restrict onto the n -dimensional manifold $\phi = 0$. However this seems unrealistic since the new difficulty is at points where Q degenerates ($\det(Q) = 0$). The density may become unbounded.

Our new idea to resolve the multivalued density in the physical space is to filter its value in phase space (x, p) onto the manifold $\phi = 0$, i.e., for any x we compute

$$\bar{\rho}(x, t) = \int \rho(t, x, p) J(t, x, p) \delta(\phi) dp,$$

where

$$J := |\det(\nabla_p \phi)| = |\det(Q)|.$$

In other words if we define a distribution function as

$$\eta(t, x, p) := \rho(t, x, p) J(t, x, p) \delta(\phi),$$

then we compute

$$(2.7) \quad \int_{\mathbb{R}^n} \eta(t, x, p) dp.$$

The above ansatz suggests that we just need to compute a new quantity

$$(2.8) \quad f(t, x, p) := \rho(t, x, p) J(t, x, p),$$

which actually solves the Liouville equation

$$(2.9) \quad \partial_t f + p \cdot \nabla_x f - \nabla_x V \cdot \nabla_p f = 0,$$

subject to the initial condition

$$f_0 = \rho_0(x) J_0(x, p),$$

where $J_0 = 1$ if $\phi_0 = p - \nabla_x S_0$ is smooth, and $J_0 = |\det(Q_0(x, y))|$ for ϕ_0 chosen otherwise. With this new quantity the singularities in density ρ are canceled out by the zeros of $J(\phi)$! *This is one of the main results in this paper.*

We now turn to justify the claim (2.9). Note that equation (2.9) is linear and homogeneous, therefore it suffices to show (2.9) for (2.8) with $J = \det(Q)$. By taking the gradient of (2.3) with respect to p we obtain the following equation for $Q = \nabla_p \phi$

$$\partial_t Q + p \cdot \nabla_x Q - \nabla_x V \cdot \nabla_p Q = -\nabla_x \phi.$$

Multiplying this equation by Q^{-1} on the left and taking the trace of the resulting equation we obtain

$$(2.10) \quad \partial_t J + p \cdot \nabla_x J - \nabla_x V \cdot \nabla_p J = -J \text{Tr}(Q^{-1} \nabla_x \phi),$$

where we have used the fact that for $J = \det(Q)$ the following holds:

$$(2.11) \quad \{\partial_t, \nabla_{x,p}\} J = J \text{Tr}(Q^{-1} \{\partial_t, \nabla_{x,p}\} Q).$$

Therefore $J \times (2.6) + \rho \times (2.10)$ gives the equation for $f = \rho J$ as claimed in (2.9).

According to a classical matrix decomposition in linear algebra, the real matrix Q can be decomposed into a product $Q = PR$ of an orthogonal matrix

P and an upper triangular matrix R . We thus have $J = \det(Q) = \det(R)$ since $P^T \cdot P = I$. Also we have

$$Q^{-1}\partial_t Q = R^{-1}\partial_t R + R^{-1}P^T\partial_t PR,$$

which gives $Tr(Q^{-1}\partial_t Q) = Tr(R^{-1}\partial_t R)$ since

$$Tr(R^{-1}P^T\partial_t PR) = Tr(P^T\partial_t P) = \frac{1}{2}Tr(P^T\partial_t P + \partial_t P^T P) = 0.$$

It suffices to prove (2.11) for upper-triangular matrix R , i.e.,

$$J^{-1}\{\partial_t, \nabla_{x,p}\}J = Tr(R^{-1}\{\partial_t, \nabla_{x,p}\}R) = \sum_{k=1}^n \{\partial_t, \nabla_{x,p}\}R(k,k)/R(k,k),$$

which can be readily verified via a direct calculation.

Finally, let us go back and take a closer look at the distribution function η . Since both ϕ and f solve the Liouville equation, so does $\delta(\phi)$ and the product $\eta = f\delta(\phi)$. For smooth initial velocity the density distribution η evolves according to

$$(2.12) \quad \partial_t \eta + p \cdot \nabla_x \eta - \nabla_x V \cdot \nabla_p \eta = 0,$$

$$(2.13) \quad \eta(0, x, p) = \rho_0(x)\delta(p - u_0(x)).$$

This recovers the semiclassical limit of the Schrödinger equation (1.1) with initial data (1.2), as $\varepsilon \rightarrow 0$, obtained via the Wigner distribution. Thus our approach provides an alternative numerical method for (2.12) that produces higher quality results. A comparison between these two approaches will be carried out in the next section.

To recover the physical observables we just need to take moments. For examples, the first two moments give the density and flux:

$$\bar{\rho} = \int \eta dp, \quad \bar{\rho u} = \int p \eta dp.$$

The density evaluated this way is the same as that obtained from formula (2.7). Higher moments can be defined in the fashion by using η .

3. NUMERICAL IMPLEMENTATION AND RESULTS

In this section we will discuss the numerical procedures of the new level set method, and present several numerical examples. For clarity in presentation involving grid indices, we shall use Φ to denote the vector valued level set function that is previously denoted as ϕ .

3.1. Numerical procedure. Let us summarize the exposition above by enumerating the numerical procedures needed for computing the density $\bar{\rho}$ and higher moment physical observables.

- (1) Initialize: construct the level set functions $\Phi_0 = (\phi_i^{(0)})$ that embed the initial data S_0 , $\nabla_x S_0$, and the phase space density function f_0 defined by (2.8) from ρ_0 in phase space.
- (2) Evolve the Liouville equation in phase space using $\phi_i^{(0)}$ and f_0 constructed above as initial conditions:

$$w_t + p \cdot \nabla_x w - \nabla_x V \cdot \nabla_p w = 0,$$

with $w(x, p, t = 0) = \phi_i^{(0)}$, $i = 1, \dots, d$, and f_0 respectively.

- (3) Evaluate $\bar{\rho}$ and other higher moments of f . The total density is obtained by integration of f along $\{p \in \mathbb{R}^d : \Phi(x, p) = 0\}$:

$$\bar{\rho}(x) = \int_{\mathbb{R}^d} f(x, p, t) \delta(\Phi(x, p)) dp,$$

and the momentum is determined by

$$\bar{\rho u}(x) = \int_{\mathbb{R}^d} p f(x, p) \delta(\Phi(x, p)) dp,$$

where $\delta(\Phi) := \prod_{i=1}^n \delta(\phi_i)$ with ϕ_i being the i^{th} component of Φ . The averaged velocity may be obtained as $\bar{\rho u} / \bar{\rho}$. If higher moments are needed, we just evaluate similar integrals with the corresponding higher powers of p .

For completeness, we describe the numerical procedures needed to evolve the Liouville equations (Steps 1 and 2). The readers can find more detailed presentations in [22] and [4] for Step 2. We leave the discussion of Step 3 to the next subsection. Also, we shall focus our discussion on the case of using a uniform Eulerian grid over $\Omega = \Omega_x \times \Omega_p \subset \mathbb{R}^d$. For $d = 2$ or 4, it is possible to perform computations on a uniform grid as described using desktop PCs, and this is what we did in order to obtain our results. However, our algorithm is valid for any $d = 2k$, $k \in \mathbb{N}$. Indeed, for $d \geq 4$, some localized algorithms should be adopted, and we will comment on this aspect at the end of this subsection.

Step 1. We need to embed the initial data as the kernel of suitable level set functions in \mathbb{R}^{2d} . If $\nabla_x S_0$ is continuous, we construct each component of Φ by

$$\phi_i(x, p, 0) = p_i - \partial_{x_i} S_0(x, 0), \quad i = 1, \dots, d,$$

where $p_i, x_i \in \mathbb{R}$ are the components of $p = (p_i) \in \mathbb{R}^d$, $x = (x_i) \in \mathbb{R}^d$. The kernel of Φ or the intersection of the zero level sets of ϕ_i determines the desired d -dimensional manifold. Otherwise we take $\phi_i(x, p, 0) = d_i(x, p)$

where $d_i(x, p)$ denotes the signed distance function to the manifold $p_i = \nabla_{x_i} S_0(x)$, component-wise, as suggested in [31].

Step 2. To solve the Liouville equation

$$\phi_t + p \cdot \nabla_x \phi - \nabla_x V \cdot \nabla_p \phi = 0,$$

we discretize the gradients $\nabla_x \phi$ and $\nabla_p \phi$ by upwinding with a fifth order WENO approximation [14]. We then discretize time by either the 3rd order TVD Runge-Kutta scheme of [25] or 4th order SSP Runge-Kutta scheme of [27]. At the boundary of our computational domain, we use a Neumann boundary condition. The corresponding CFL condition for the Liouville equations is:

$$\Delta t \leq \frac{\Delta x}{2 \max_{(x,p) \in \Omega} (p, \nabla_x V)}.$$

Before we can actually evolve the system numerically, we need to determine the computational domain for the problem. It is clear that we are flowing a Hamiltonian system, and thus the total energy $H(x(t), p(t))$ is invariant under the flow. More precisely, for $t \geq 0$, $(x(t), p(t))$ stays on the invariant manifold \mathcal{M}_0 , which is the H_0 level set of the Hamiltonian H determined by the initial data (x_0, p_0) . Furthermore, by definition, \mathcal{M}_0 is a closed submanifold in the phase space (in this paper, we consider either \mathbb{R}^2 or \mathbb{R}^4). Hence, the range of (x, p) is determined by the given initial data and the Hamiltonian.

Let us illustrate this by an example in \mathbb{R}^2 with the inhomogeneous Hamiltonian $H(x, p) = (p^2 + x^2)/2$. With the initial data $(x_0, p_0) = (\sqrt{2}, \sqrt{2})$, the invariant manifold $\mathcal{M}_{\sqrt{2}}$ is the two-level set of H , corresponding to the circle with radius two, centered at the origin. Therefore, the possible range of p for this system is bounded by the extrema of p constraint on the circle; in this example it is $[-2, 2]$. Correspondingly, we can determine the range of x . Of course, for our problem, we generally evaluate a system of such flows determined by $(x, \partial_x S_0(x))$, with $x \in \Omega_x$ and Ω_x compact. We then determine the range of (x, p) needed for computation by obtaining bounds determined from each energy level set $\mathcal{M}_x, x \in \Omega_x$.

For efficiency in computation, one can perform Steps 1-3 locally in an open neighborhood around the zero level sets. Indeed, in [22], the authors demonstrated this approach by adopting the local level set technique introduced in [23]. It is also possible to use a so-called semi Lagrangian method to localize the computation, see [28, 29] for codimension one calculations. However, there are extra numerical considerations on how the zero level sets of ϕ_i should intersect. In [22] and [4], the authors discussed the strategy of combining distance reinitialization (making each ϕ_i to be the signed distance function to its zero level set) and enforcing orthogonality in the

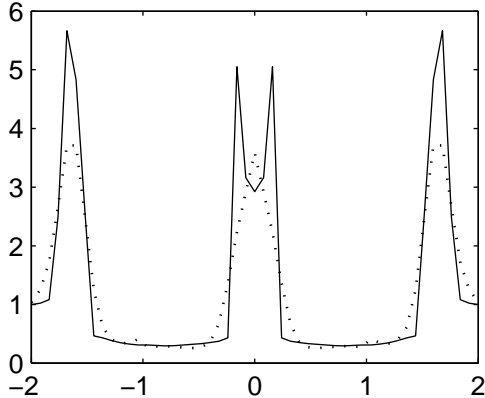


FIGURE 3.1. Comparison of the density computed from evolving the delta function initial data (dotted curve) and the proposed level set approach (solid curve). These are numerical solutions to the problem described in Example 3.2.

pair-wise intersection of the zero level sets of ϕ_i . We refer the detailed discussion to those two papers. We point out, however, that this strategy will affect the evaluation of the density integral. The changes in the gradients of ϕ_i resulting from these operations require recomputations of f . We will discuss more details related to this in a future paper.

We remark that it is also possible to obtain the physical observables by evolving a single Liouville equation with the initial condition containing δ -functions.

$$\eta_t + p \cdot \nabla_x \eta - \nabla_x V \cdot \nabla_p \eta = 0,$$

with

$$\eta(x, p, t = 0) = \rho_0(x) \delta(p - \nabla_x S_0).$$

However, this approach is not appropriate as a numerical device, since numerical viscosity would smear out the δ function and degenerate the accuracy at the integration needed for total density computation. In addition, the corresponding methods for local computations have not been extensively studied. Figure 3.1 shows a comparison of such approach to our level set approach. The computation of the Liouville equation is done as we suggested above, using upwinding and the 5th order WENO spatial discretization. With exactly the same grid, one sees in the figure that the result obtained from tracking the δ initial data is inferior to the level set result.

Finally, we point out a valuable tool developed in [21] for explicit approximation of the phase gradient location from the given level set function Φ and for visualization. The same author is currently developing a high codimension semi-Lagrangian method which looks quite promising.

3.2. On numerical integration of the moments. In the evaluation of the density integral

$$(3.1) \quad \bar{\rho}(x, t) = \int_{\mathbb{R}^d} f(x, p) \Pi_j \delta(\phi_j(x, p)) dp,$$

typically, one replaces the Dirac- δ distribution by an approximation δ_η , such that $\delta_\eta \rightarrow \delta$ as $\eta \rightarrow 0+$. Common choices of δ_η range from a normalized Gaussian to compactly supported kernels with $2\eta > 0$ denoting the support size. Integral (3.1) is then approximated by a Riemann sum over a uniform grid with mesh size h . For example, for $d = 2$, we have:

$$\bar{\rho}_{h,\eta}(x, t) = \sum_{i,j} h^2 f(x, p_{i,j}, t) \delta_\eta(\phi_1(x, p_{i,j}, t)) \delta_\eta(\phi_2(x, p_{i,j}, t));$$

here $\bar{\rho}$ is a function of two spatial dimensions. One concludes that

$$\bar{\rho} = \lim_{\eta \rightarrow 0+} \lim_{h \rightarrow 0+} \bar{\rho}_{h,\eta},$$

if the limits are evaluated in the order as above. However, in actual numerical computation, it is important to compute convergent approximations of (3.1) as $h \rightarrow 0$ efficiently and with good quality for a given range of grid sizes, i.e. small error relative to the grid size. A common practice is to put the amount of regularization η , here corresponding to the support size, as a function of h such that $\eta(h) \rightarrow 0+$ as $h \rightarrow 0+$. However, it is not obvious that $\rho_h = \rho_{h,\eta(h)}$ converges to $\bar{\rho}$. In our study, we found that it is essential to sample δ_η correctly over the grid. This amounts to the correct selection of the kernel δ_η and the regularization parameter η *in relation to both the given grid geometry, and the gradient of the level set functions.*

We will use the simple piecewise linear kernel

$$\delta_\eta^{(1)}(x) = \begin{cases} \frac{1}{\eta} \left(1 - \frac{|x|}{\eta}\right), & |x| \leq \eta \\ 0, & |x| > \eta \end{cases}$$

to illustrate our reasoning. First, the delta function needs to be resolved by the grid. Let $x_j = jh$ denote the grid points. If we choose an $\eta_0(h)$ smaller than the grid size, it is obvious that $\delta_{\eta_0(h)}^{(1)}$ is equivalent to 0 on the grid, regardless of the grid size. Thus $\eta(h) \geq h$. Since the integrals of interest in this paper involve the composition of δ -function and a level set function, we need to study the scaling of the regularization under this composition. Let $\phi(x)$ be the one dimensional level set function: $\phi(x) = px$, $p > 0$. Let $z_j = \phi(x_j) = p \cdot jh$. We immediately realize that $\eta(h)$ has to be greater than ph in order for the discretization to take effect; i.e. *the amount of regularization should be an increasing function of the gradient of the level set function!* We remark that some of the related aspects are extensively studied in the papers [30], and in particular, related to level set methods

in [9]. Their results suggest that special techniques are needed in order to avoid grid effects that result in $O(1)$ error regardless of grid refinement. It is pointed out in [30] that if η is chosen to be positive integer multiple of h , $\kappa_0 h$, then $\delta_\eta^{(1)}(x)$ as well as the cosine kernel

$$\delta_\eta^{(2)}(x) = \begin{cases} \frac{1}{2\eta}(1 + \cos \frac{\pi x}{\eta}), & |x/\eta| \leq 1 \\ 0, & |x/\eta| > 1 \end{cases}$$

have the so-called ‘‘exact integration property’’, meaning

$$\sum_{j=-N}^N \delta_{\kappa_0 h}^{(k)}(x_j - x_0)h = 1, \text{ for any } -Nh < x_0 < Nh, k = 1, 2.$$

In our simulations, we use $\delta_\eta^{(2)}(x)$ and scale η with $|\phi_p|$ by

$$\eta(h, |\phi_p|) = 2 \max(|\phi_p|, 1) \cdot h.$$

Here, $|\phi_p|$ denotes the Jacobian of $\Phi = (\phi_j)$ with respect to p :

$$|\partial\Phi/\partial(p_1, \dots, p_d)|,$$

and is approximated by central differencing. Figure 3.2 is a comparison using additional scaling factors. In higher dimensions ($d \geq 2$), [9] suggests the possibility of subtle complications related to the grid effects. This means that the regularization parameter η should also depends on $\nabla_{x,p}\phi_j$, $j = 1, \dots, d$. In our computations, we either use the same scaling as described above or perform distance reinitializations together with orthogonality adjustments on ϕ_j , as suggested in [4, 22], and recompute f due to the change in $|\partial\Phi/\partial(p_1, \dots, p_d)|$ and finally scale η as suggested. We shall present more study of various related aspects in a forthcoming paper.

We remark that not all approximate delta functions satisfy the exact integration property. Moreover, even if the kernel is chosen to be either $\delta_\eta^{(1)}$, $\delta_\eta^{(2)}$, or one with many vanishing moments, if η is chosen carelessly, one typically will get a small error that does not vanish as $h \rightarrow 0$. Our experience suggests that, in general, the scaling similar to $\eta(h) = \sqrt{h}$ should be used for convergence. To see this, consider the periodic extension of $f(x)\delta_\eta(x)$, where $\delta(x)$ is supported in $[-1, 1]$ and $\delta_\eta(x) = \delta(x/\eta)/\eta$. Furthermore, let $S = \int_{\mathbb{R}} f(x)\delta(x)dx = f(0)$, $I_\eta = \int_{[-\eta, \eta]} f(x)\delta_\eta(x)dx$ and S_h be the corresponding Riemann sum with mesh size h . We see that the error can be formally bounded by

$$|S_h - S| \leq |S_h - I_\eta| + |I_\eta - S|.$$

Now consider the cosine kernel, $\delta_\eta^{(2)}$, and assume that f is a smooth function. Then we know that the periodic extension of $f(x)\delta_\eta^{(2)}(x)$ is a C^2 function on \mathbb{R} , and thus the quadrature error is bounded by

$$|\mathcal{S}_h - I_\eta| \leq C_0\eta \cdot \frac{d^2}{dx^2}(f(x)\delta_\eta^{(2)}(x)) \leq \tilde{C}_0 \frac{h^2}{\eta^2}.$$

Since $\delta_\eta^{(2)}$ has one vanishing moment, $|I_\eta - \mathcal{S}| \leq C_1\eta^2$. Hence, by choosing $\eta = \sqrt{h}$, the optimal error bound

$$|\mathcal{S}_h - \mathcal{S}| \leq h$$

is achieved. The scaling of this kind raises the question about the quality of solution for real computations. Clearly, the \sqrt{h} -scaling on the support size implies excessive smearing with respect to the given grid configuration. Moreover, in the above context, it imposes a condition on the size of the grid; i.e. there should always be $C_0h^{-1/2}$ grid points near the location of the point mass, x_0 . In our case, this translates to the restriction of the mesh size in relation with the diameter of each connected component of $\{p : \phi(x, p) < 0\}$ for each x . There is yet another disadvantage of using kernels with higher moment conditions, and it stems from the particular shapes of $\bar{\rho}$. At each ‘‘overturning’’ of the gradients $\nabla_x \mathcal{S}$, $\bar{\rho}$ develops a singularity, which is numerically realized as a narrow peak. Higher order kernels typically result in small oscillations near such kind of peak. This is, to certain level, related to the interpolation of discontinuous functions using a smooth basis. Figure 3.3 shows a comparison of a computation done using a fourth order kernel to that from the cosine kernel. The result obtained from using a 4th order kernel is much more smeared out and contains oscillations that do not go away even after grid refinement.

3.3. Numerical examples.

Example 3.1. 1D free motion ($V = 0$). $u_0(x) = -\sin(\pi x)|\sin(\pi x)|$, and $\rho_0(x) = \exp(-(x - 0.5)^2)$.

This example is taken from [13]. Figures 3.2, 3.3, and 3.4 contain results using this example. Notice that in Figure 3.4, the averaged velocity \bar{u} , defined in (1.15), is plotted against the multivalued velocity, and they values are equal wherever the system does not develop multivalued solution.

Example 3.2. 1D free motion ($V=0$)

$$S_0(x) = -\alpha(\ln(\cosh(x - \beta)) + \ln(\cosh(x + \beta))), \text{ and } \rho_0(x) = 1.$$

Figure 3.5 shows a progression of velocity and the corresponding density. We run our algorithm on a succession of mesh sizes of the same problem

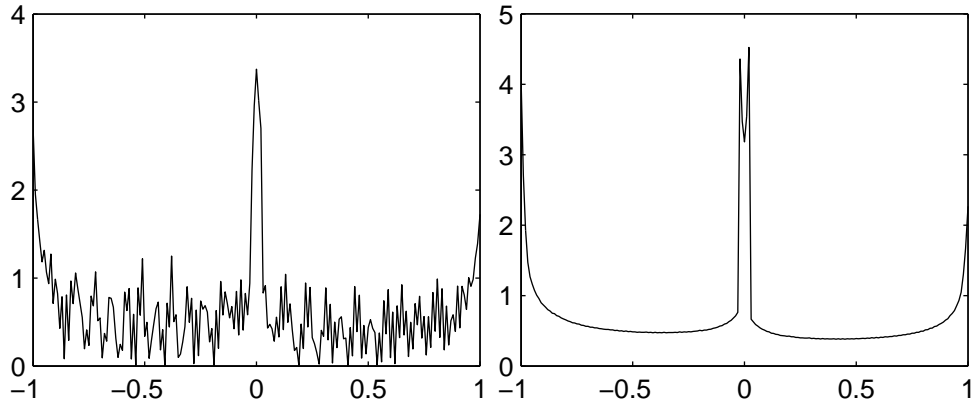


FIGURE 3.2. A numerical study of the regularization of the δ function. The plot on the left is the density obtained from using a support size that is constant multiple of the grid size. The right one is the density integral evaluated with the proposed scaling. These are numerical solutions to the problem described in Example 3.1.

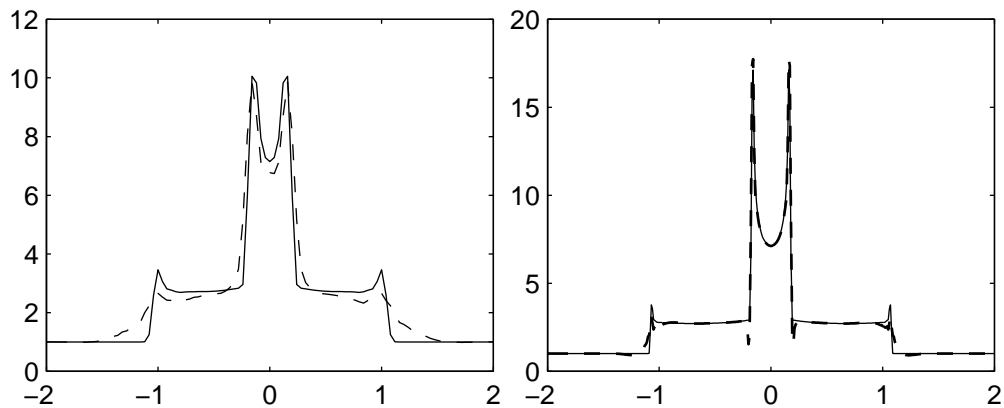


FIGURE 3.3.

The dashed lines are the density computed by using the fourth order kernel. The solid lines are the result obtained from using the cosine kernel. The grid sizes are respectively 100 and 400. These are numerical solutions to the problem described in Example 3.1.

with $\alpha = 0.75$ and $\beta = 1.0$. One result is shown in Figure 3.6. Figures 3.7 and 3.8 show some 4D computational results using $\alpha = 0.5$ and $\beta = 1.0$.

Example 3.3. Consider the 1-D model with periodic potential $V(x) = \cos(2x + 0.4)$

$$S_0(x) = \sin(x + 0.15),$$

$$\rho_0(x) = \frac{1}{2\sqrt{\pi}} \left[\exp\left(-\left(x + \frac{\pi}{2}\right)^2\right) + \exp\left(-\left(x - \frac{\pi}{2}\right)^2\right) \right].$$

Figure 3.9 shows a progression in time of the velocity and the corresponding density. The velocity eventually develop some small details that require a finer grid to resolve. Figure 3.10 shows a plot at a later time for this system. In this figure, we also plotted the averaged velocity, and as a function of x , it has discontinuities where $\phi_p = 0$.

Example 3.4. A radial symmetric two dimensional test problem: $\phi_0(x_1, x_2) = 0.5(1 - r^2)$, where $r^2 = x_1^2 + x_2^2$. $V(x) = 0$.

The averaged density function is plotted at $T = 1.0$ and 1.25 . See Figure 3.11.

Example 3.5. Consider a 2-D model with a quadratic potential (Harmonic oscillator $V = |x|^2/2$).

$$(3.2) \quad S_0(x_1, x_2) = 0.6(\sin(0.4\pi x_1) - 0.1)(\sin(0.4\pi x_2) - 0.2),$$

$$(3.3) \quad \rho_0(x) = \exp(-|x|^2) + 1.0.$$

Figure 3.12 shows the averaged density of the system at time $T = 8.0$ and Figure 3.13 shows the contour plots of the components of the averaged velocity.

4. CONCLUSION

We introduce a new level set method for computing the multivalued density and other physical observables for the semiclassical limit of the Schrödinger equation. The proposed method is built upon our previous approach for computing the phase gradients [4, 16, 22]. Compared to the moment methods that are constrained by a predetermined number of multivalued branches, our approach automatically computes all the branches that occur in the system. Furthermore, instead of solving a system of weakly hyperbolic equations, as in the moment methods, which require delicate computations, we solve a linear convection equation that generalizes easily to any number of dimensions. What is new to our previous approach, and also to other methods, is in the moment (density, momentum, etc.) calculation. The density is computed by evolving the same linear equation with smooth initial data, and all of the moments can then be evaluated by integration in the phase directions along the bicharacteristics strip only at the time needed. We do not track any singular quantities that might require extra

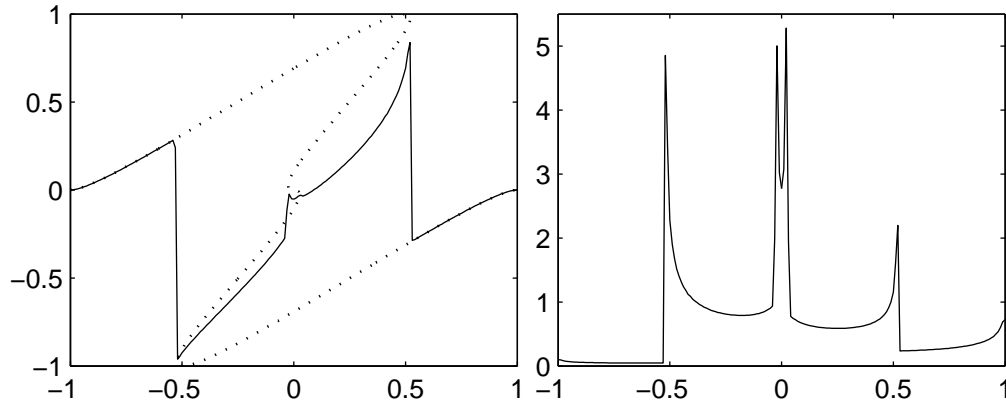


FIGURE 3.4. 200 grid points is used. In the plot on the left, the multivalued velocity is shown as the dotted curve against the average velocity in solid curve. On the right is the corresponding density $\bar{\rho}$.

grid resolution and might result in oscillation or excessive smearing. With our numerical treatment of the last integration step, the sharp result can be obtained efficiently.

The applications of the method are not restricted to the computation of the semiclassical limits of the Schrödinger equations. Similar problems arise in geometrical optics, seismic imaging and multiple arrivals where the computation of multivalued solutions are essential. The techniques discussed in this paper are naturally geometrical and very well suited for handling multivalued solutions.

APPENDIX

In this appendix we provide an alternative justification of the level set method introduced.

Consider the initial value problem for the Liouville equation

$$(4.1) \quad \partial_t w + pw_x - V_x w_p = 0,$$

$$(4.2) \quad w(0, x, p) = \rho_0(x) |\partial_p \phi_0(x, p)| \delta(\phi_0(x, p)).$$

Recall that the problem we want to solve, the semiclassical limit of the Schrödinger equation (1.1) with initial data (1.2), is the case when $\phi_0(x, p) = p - u_0(x)$ for continuous $u_0(x)$, or ϕ is the signed distance function for discontinuous u_0 .

Introduce the Hamiltonian flow,

$$(4.3) \quad \begin{cases} x'(t) &= p, & x(0) &= x_0, \\ p'(t) &= -V_x(x); & p(0) &= p_0. \end{cases}$$

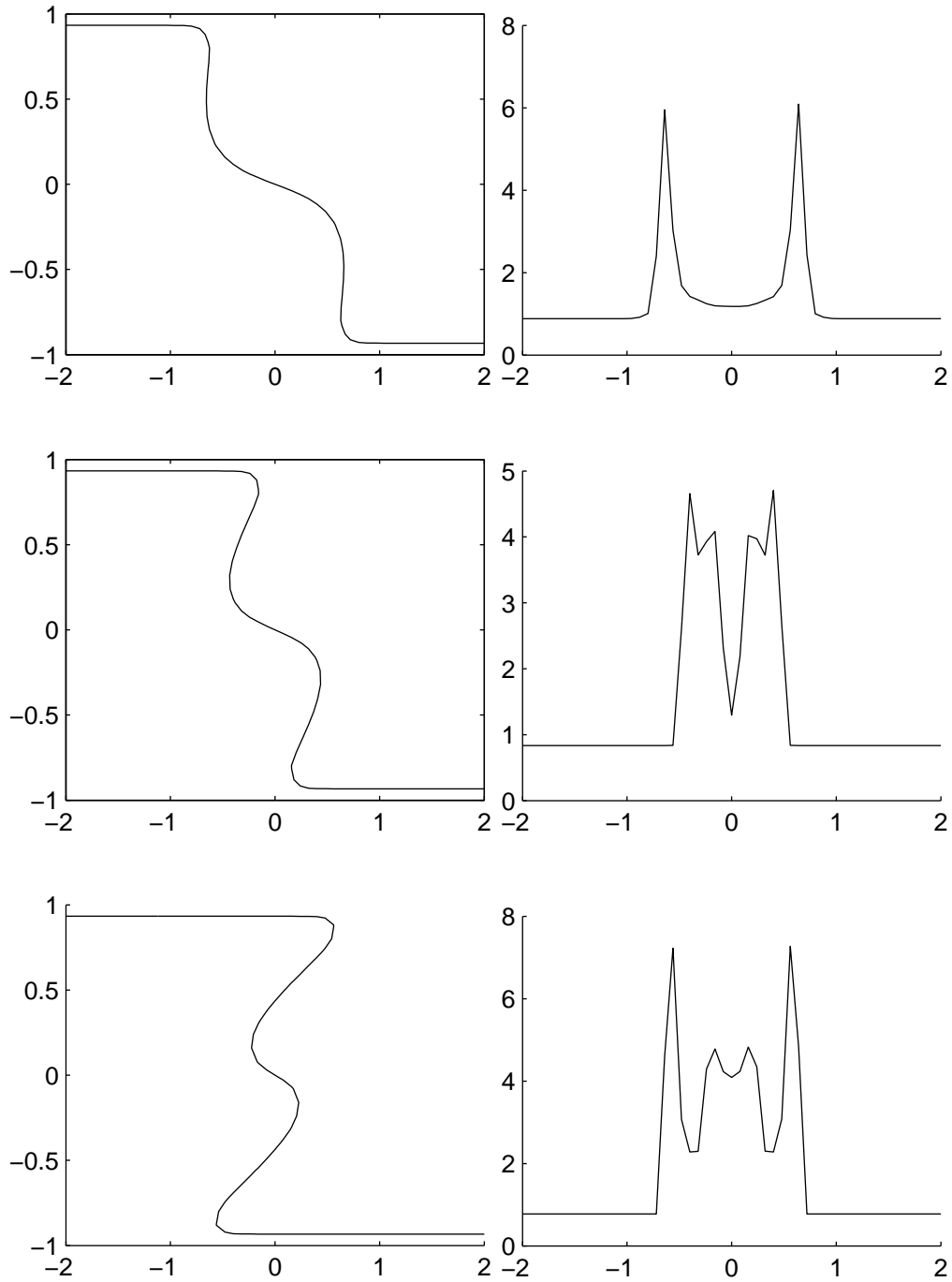


FIGURE 3.5. 5-folding in the velocity (the left cloumn) and the corresponding averaged density (the right column). 50 grid points are used in our computation, and the results are plotted at $T = 3.5, 5.0$, and 7.5 .

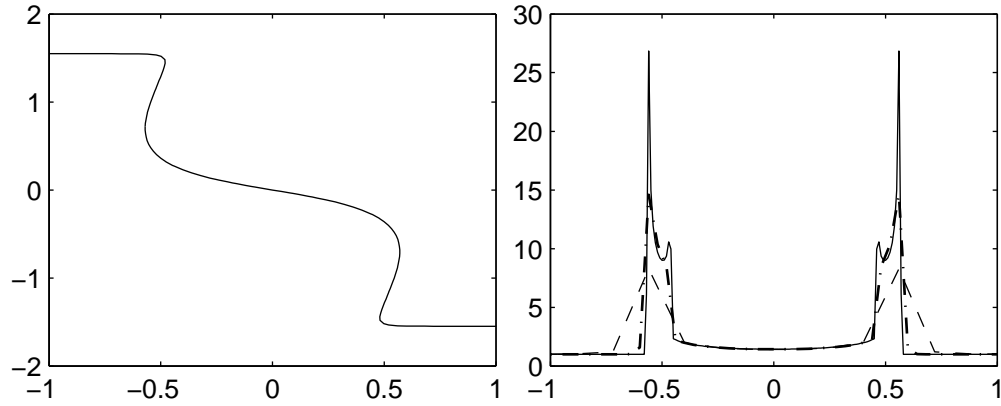


FIGURE 3.6. A numerical convergence study. The density function $\bar{\rho}$ is plotted at $T = 3.2$ using different grid sizes. The the fi gure on the left shows the multiple branches of the velocity. In fi gure on the right, the dashed line corresponds to $h = 0.16$; The dash-dotted line ($h = 0.04$); and the solid line($h = 0.01$).

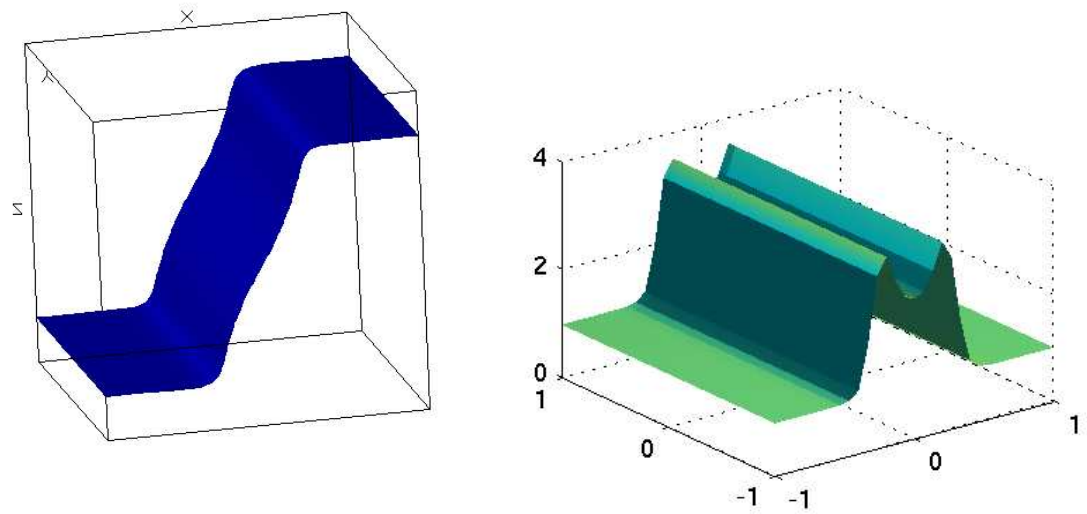


FIGURE 3.7. Example 3. 30 grid points in each dimension. $T = 0.99$. The plot on the left is the velocity, the plot on the right is the density computed.

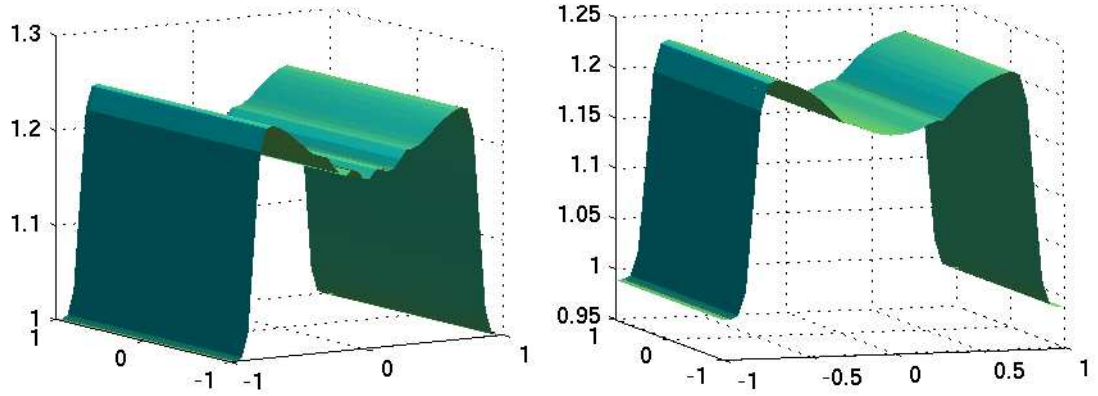


FIGURE 3.8. The plot on the left is the density computation with bad scaling. One can see the oscillations.

We denote the solution to these ODEs by $x = x(t, x_0, p_0)$ and $p = p(t, x_0, p_0)$. The curves (x, p) are the *bicharacteristics* in phase space. Assume V is smooth. Since the Hamiltonian flow is volume preserving, the bicharacteristic curves defined by (4.3) are invertible and we denote the inverse functions by $(x_0(t, x, p), p_0(t, x, p))$. Since the solution of the Liouville equation (4.1) is a constant along the bicharacteristic curve defined by (4.3), we have

$$\begin{aligned}
 (4.4) \quad w(t, x, p) &= w(0, x_0(t, x, p), p_0(t, x, p)) \\
 &= \rho_0(x_0) |\partial_p \phi_0(x_0, p_0)| \delta(\phi_0(x_0, p_0))
 \end{aligned}$$

We now consider the following two problems.

$$(4.5) \quad \partial_t f + p \cdot f_x - V_x \cdot f_p = 0,$$

$$(4.6) \quad f(0, x, p) = \rho_0(x) |\partial_p \phi_0(x, p)|;$$

$$(4.7) \quad \partial_t \phi + p \cdot \phi_x - V_x \cdot \phi_p = 0,$$

$$(4.8) \quad \phi(0, x, p) = \phi_0(x, p).$$

The exact solution to these two problems are

$$(4.9) \quad f(t, x, p) = \rho_0(x_0) |\partial_p \phi_0(x_0, p_0)|$$

$$(4.10) \quad \phi(t, x, p) = \phi_0(x_0, p_0)$$

So clearly, by comparing (4.4) with (4.9), (4.10), we have

$$(4.11) \quad w(t, x, p) = f(t, x, p) \delta(\phi(t, x, p)).$$

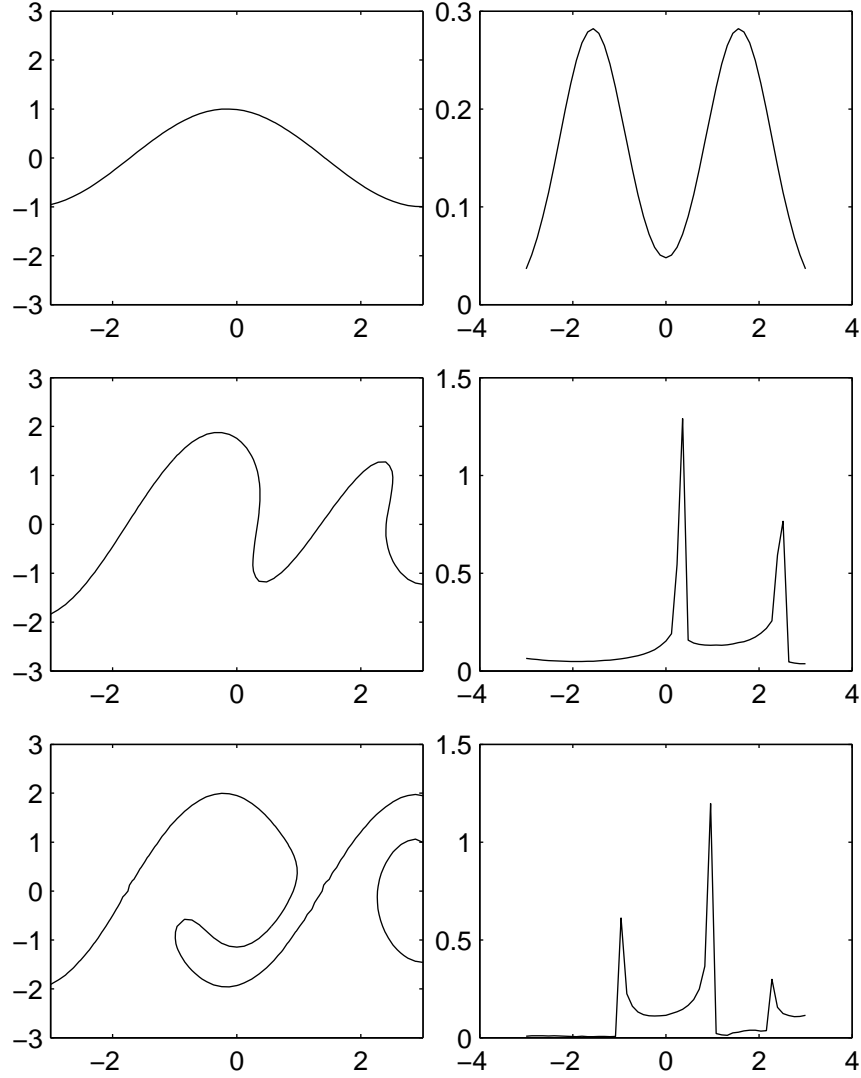


FIGURE 3.9. Example 3.3. 50 grid points over $[-3, 3]$. The left column shows the multivalued phase gradients at time $T = 0.0, 6.0,$ and 12.0 . The right column shows the corresponding density.

The physical observables of the Liouville equation (4.1) are thus given by

$$(4.12) \quad \bar{p} = \int w dp = \int f(t, x, p) \delta(\phi(t, x, p)) dp,$$

$$(4.13) \quad \overline{p\bar{u}} = \int p w dp = \int p f(t, x, p) \delta(\phi(t, x, p)) dp.$$

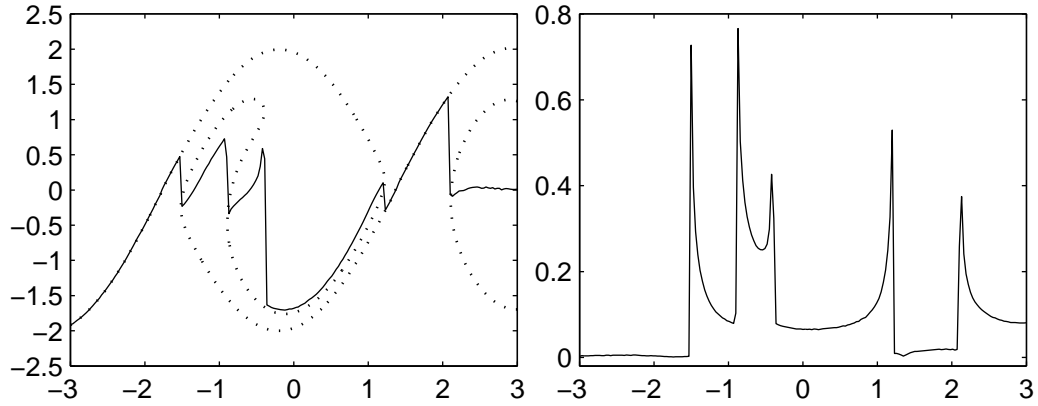


FIGURE 3.10. 200 grid points are used. The dotted line and the solid line in the plot on the left correspond respectively to the multivalued phase gradient and its average (\bar{u}). The plot on the right is the corresponding density $\bar{\rho}$ at $T = 18.0$.

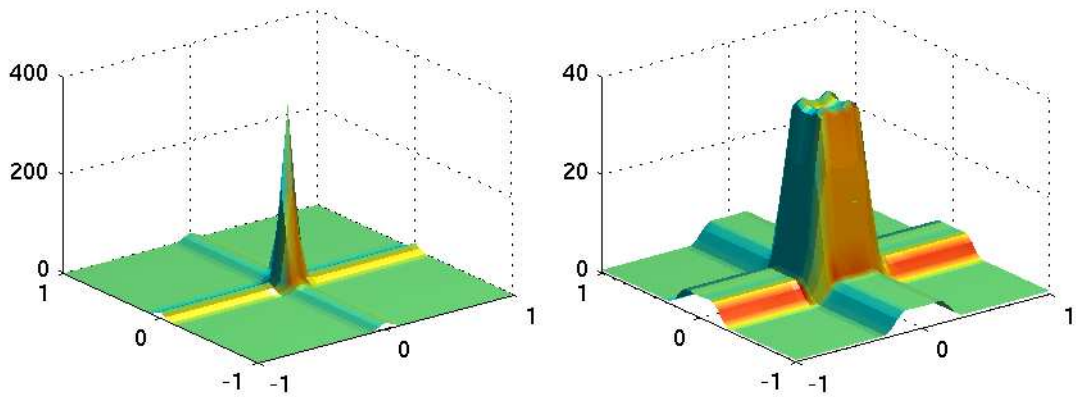


FIGURE 3.11. $T = 1.0$ and 1.25 . 40 grid points.

ACKNOWLEDGMENTS

Jin's research was supported in part by the National Science Foundation under Grant DMS0305080. Liu's research was supported in part by the National Science Foundation under Grant DMS01-07917. Osher's research was supported by AFOSR Grant F49620-01-1-0189. Tsai's research is supported in part by the National Science Foundation under agreement No. DMS-0111298. Any opinions, findings and conclusions or recommendations expressed in this material are those of the authors and do not necessarily reflect the views of the National Science Foundation.

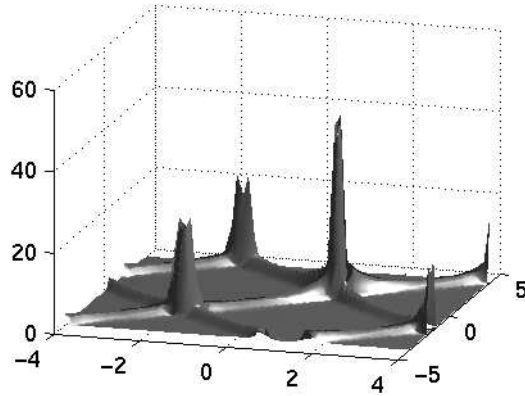


FIGURE 3.12. Averaged density of Example 3.5 at $T = 6.7$.

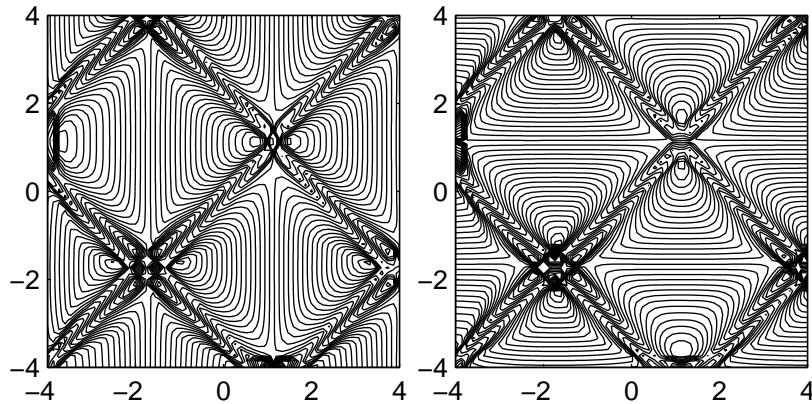


FIGURE 3.13. Averaged velocity of Example 3.5 at $T = 6.7$. Here the contour plots of $\bar{u} = (\bar{u}_1, \bar{u}_2)$ are shown.

The last author thanks Bjorn Engquist for many useful conversations.

REFERENCES

- [1] W.Z. Bao, S. Jin, and P.A. Markowich. On time-splitting spectral approximations for the Schrödinger equation in the semiclassical regime. *Journal of Computational Physics*, 175:487–524, 2002.
- [2] Y. Brenier and L. Corrias. A Kinetic Formulation for Multi-Branch Entropy Solutions of Scalar Conservation Laws. *Ann. IHP Analyse non-linéaire*, 1996.
- [3] Y. Brenier and E. Grenier. Sticky particles and scalar conservation laws. *SIAM J. Numer. Anal.*, 35(6):2317–2328 (electronic), 1998.
- [4] Li-Tien Cheng, Hailiang Liu, and Stanley Osher. Computational high-frequency wave propagation using the level set method, with applications to the semi-classical limit of Schrödinger equations. *Comm. Math. Sci.*, 1(3):593–621, 2003.

- [5] Li-Tien Cheng, Stanley Osher, Myungjoo Kang, Hyeseon Shim, and Yen-Hsi Tsai. Reflection in a level set framework for geometric optics. *Computer Methods in Engineering and Physics*, 2003. to appear.
- [6] Michael G. Crandall and Pierre-Louis Lions. Viscosity solutions of Hamilton-Jacobi equations. *Trans. Amer. Math. Soc.*, 277(1):1–42, 1983.
- [7] Björn Engquist and Olof Runborg. Multi-phase computations in geometrical optics. *J. Comput. Appl. Math.*, 74(1-2):175–192, 1996. TICAM Symposium (Austin, TX, 1995).
- [8] Bjorn Engquist and Olof Runborg. Computational high frequency wave propagation. In *Acta numerica, 2003*, Acta Numer. Cambridge Univ. Press, Cambridge, 2003.
- [9] Bjorn Engquist, Anna-Karin Tornberg, and Yen-Hsi Tsai. Dirac- δ functions in level set methods. 2003. In preparation.
- [10] Ingenuin Gasser and Peter A. Markowich. Quantum hydrodynamics, Wigner transforms and the classical limit. *Asymptot. Anal.*, 14(2):97–116, 1997.
- [11] Patrick Gérard, Peter A. Markowich, Norbert J. Mauser, and Frédéric Poupaud. Homogenization limits and Wigner transforms. *Comm. Pure Appl. Math.*, 50(4):323–379, 1997.
- [12] Laurent Gosse. Using K -branch entropy solutions for multivalued geometric optics computations. *J. Comput. Phys.*, 180(1):155–182, 2002.
- [13] Laurent Gosse, Shi Jin, and Xiantao Li. On two moment systems for computing multiphase semiclassical limits of the Schrödinger equation. 2003. To appear, *Math. Model Methods in Appl. Sci.*
- [14] Guang-Shan Jiang and Danping Peng. Weighted ENO schemes for Hamilton-Jacobi equations. *SIAM J. Sci. Comput.*, 21(6):2126–2143 (electronic), 2000.
- [15] Shi Jin and Xiantao Li. Multi-phase computations of the semiclassical limit of the Schrödinger equation and related problems: Whitham Vs Wigner. *Physica D*, 182:46–85, 2003.
- [16] Shi Jin and Stanley Osher. A level set method for the computation of multivalued solutions to quasi-linear hyperbolic PDE’s and Hamilton-Jacobi equations. *Comm. Math. Sci.*, 1(6):575–591, 2003.
- [17] X. Li, J.G. Wöhlbier, S. Jin, and J.H. Booske. An Eulerian method for computing multi-valued solutions of the Euler-Poisson equations and applications to wave breaking in klystrons. 2003. Submitted to *Physical Review E*.
- [18] Pierre-Louis Lions and Thierry Paul. Sur les mesures de Wigner. *Rev. Mat. Iberoamericana*, 9(3):553–618, 1993.
- [19] Hailiang Liu, Li-Tien Cheng, and Stanley Osher. A level set framework for tracking multi-valued solutions to nonlinear first-order equations. 2003. Preprint.
- [20] P.A. Markowich, P. Pietra, and C. Pohl. Numerical approximations of quadratic observables of Schrödinger-type equations in the semiclassical limit. *Numer. Math.*, 81:595–630, 1999.
- [21] Chohong Min. Simplicial isosurfacing in arbitrary dimension and codimension. *J. Comput. Phys.*, 190:295–310, 2003.
- [22] Stanley Osher, Li-Tien Cheng, Myungjoo Kang, Hyeseon Shim, and Yen-Hsi Tsai. Geometric optics in a phase-space-based level set and Eulerian framework. *J. Comput. Phys.*, 179(2):622–648, 2002.
- [23] Danping Peng, Barry Merriman, Stanley Osher, Hongkai Zhao, and Myungjoo Kang. A PDE-based fast local level set method. *J. Comput. Phys.*, 155(2):410–438, 1999.

- [24] Jianliang Qian, Li-Tien Cheng, and Stanley Osher. A level set-based Eulerian approach for anisotropic wave propagation. *Wave Motion*, 37(4):365–379, 2003.
- [25] Chi-Wang Shu and Stanley Osher. Efficient implementation of essentially nonoscillatory shock-capturing schemes. II. *J. Comput. Phys.*, 83(1):32–78, 1989.
- [26] C. Sparber, P.A. Markowich, and N. J. Mauser. Multivalued geometrical optics: Wigner functions versus WKB-methods. *Asymptotic Analysis*, 33:153–187, 2003.
- [27] R.J. Spiteri and S.J. Ruuth. A new class of optimal high-order strong-stability-preserving time discretization methods. 2001. Preprint).
- [28] John Strain. Fast tree-based redistancing for level set computations. *J. Comput. Phys.*, 152(2):664–686, 1999.
- [29] John Strain. Semi-Lagrangian methods for level set equations. *J. Comput. Phys.*, 151(2):498–533, 1999.
- [30] Anna-Karin Tornberg and Björn Enquist. Regularization techniques for numerical approximation of PDEs with singularities. *UCLA CAM Report*, 02(37), 2002. To appear, *J. Sci. Comp.*
- [31] Yen-Hsi Richard Tsai, Yoshikazu Giga, and Stanley Osher. A level set approach for computing discontinuous solutions of Hamilton-Jacobi equations. *Math. Comp.*, 72(241):159–181 (electronic), 2003.
- [32] Ya. B. Zeldovich. Gravitational instability: An approximate theory for large density perturbations. *Astron. and Astrophys.*, 5:84–89, 1970.

DEPARTMENT OF MATHEMATICS, UNIVERSITY OF WISCONSIN, MADISON, WI 53706
E-mail address: jin@math.wisc.edu

IOWA STATE UNIVERSITY, MATHEMATICS DEPARTMENT, AMES, IA 50011
E-mail address: hliu@iastate.edu

LEVEL SET SYSTEMS, INC, 1058 EMBURY STREET, PACIFIC PALISADES, CA 90272-2501
E-mail address: sjo@levelset.com

INSTITUTE FOR ADVANCED STUDY AND DEPARTMENT OF MATHEMATICS, PRINCETON UNIVERSITY, PRINCETON, NJ 08544
E-mail address: ytsai@math.ias.edu